MNRAS **470,** L11–L15 (2017)
Advance Access publication 2017 May 1
doi:10.1093/mnrasl/slx066

The angular power spectrum measurement of the Galactic synchrotron emission in two fields of the TGSS survey

Samir Choudhuri,[1,2]★ Somnath Bharadwaj,[2] Sk. Saiyad Ali,[3] Nirupam Roy,[4] Huib. T. Intema[5] and Abhik Ghosh[6,7]

[1]*National Centre For Radio Astrophysics, Post Bag 3, Ganeshkhind, Pune 411 007, India*
[2]*Department of Physics & Centre for Theoretical Studies, IIT Kharagpur, Kharagpur 721 302, India*
[3]*Department of Physics,Jadavpur University, Kolkata 700032, India*
[4]*Department of Physics, Indian Institute of Science, Bangalore 560012, India*
[5]*Leiden Observatory, Leiden University, Niels Bohrweg 2, NL-2333CA, Leiden, The Netherlands*
[6]*Department of Physics and Astronomy, University of the Western Cape, Robert Sobukwe Road, Bellville 7535, South Africa*
[7]*SKA SA, The Park, Park Road, Pinelands 7405, South Africa*

Accepted 2017 April 27. Received 2017 April 26; in original form 2016 December 20

ABSTRACT

Characterizing the diffuse Galactic synchrotron emission at arcminute angular scales is needed to reliably remove foregrounds in cosmological 21-cm measurements. The study of this emission is also interesting in its own right. Here, we quantify the fluctuations of the diffuse Galactic synchrotron emission using visibility data for two of the fields observed by the TIFR GMRT Sky Survey. We have used the 2D Tapered Gridded Estimator to estimate the angular power spectrum (C_ℓ) from the visibilities. We find that the sky signal, after subtracting the point sources, is likely dominated by the diffuse Galactic synchrotron radiation across the angular multipole range $240 \leq \ell \lesssim 500$. We present a power-law fit, $C_\ell = A \times \left(\frac{1000}{l}\right)^\beta$, to the measured C_ℓ over this ℓ range. We find that (A, β) have values $(356 \pm 109\,\mathrm{mK}^2, 2.8 \pm 0.3)$ and $(54 \pm 26\,\mathrm{mK}^2, 2.2 \pm 0.4)$ in the two fields. For the second field, however, there is indication of a significant residual point source contribution and for this field we interpret the measured C_ℓ as an upper limit for the diffuse Galactic synchrotron emission. While in both fields the slopes are consistent with earlier measurements, the second field appears to have an amplitude that is considerably smaller compared to similar measurements in other parts of the sky.

Key words: methods: data analysis – methods: statistical – techniques: interferometric – diffuse radiation.

1 INTRODUCTION

Observations of the redshifted 21-cm signal from the Epoch of Reionization (EoR) contain a wealth of cosmological and astrophysical information (Bharadwaj & Ali 2005; Furlanetto, Oh & Briggs 2006; Morales & Wyithe 2010; Pritchard & Loeb 2012). The Giant Metrewave Radio Telescope (GMRT; Swarup et al. 1991) is currently functioning at a frequency band that corresponds to the 21-cm signal from this epoch. Several ongoing and future experiments such as the Donald C. Backer Precision Array to Probe the Epoch of Reionization (PAPER; Parsons et al. 2010), the Low Frequency Array (LOFAR, van Haarlem et al. 2013), the Murchison Wide-field Array (MWA; Bowman et al. 2013), the Square Kilometre Array (SKA1 LOW; Koopmans et al. 2015) and the Hydrogen Epoch of Reionization Array (HERA; Neben et al. 2016) are aiming to measure the EoR 21-cm signal. The EoR 21-cm signal is overwhelmed by different foregrounds that are 4–5 orders of magnitude stronger than the expected 21-cm signal (Shaver et al. 1999; Ali, Bharadwaj & Chengalur 2008; Ghosh et al. 2011a,b). Accurately modelling and subtracting the foregrounds from the data are the main challenges for detecting the EoR 21-cm signal. The diffuse Galactic synchrotron emission (hereafter, DGSE) is expected to be the most dominant foreground at 10 arcmin angular scales after point source subtraction at 10–20 mJy level (Bernardi et al. 2009; Ghosh et al. 2012; Iacobelli et al. 2013). A precise characterization and a detailed understanding of the DGSE are needed to reliably remove foregrounds in 21-cm experiments. In this Letter, we characterize the DGSE at arcminute angular scales, which are relevant for the cosmological 21-cm studies.

The study of the DGSE is also important in its own right. The angular power spectrum (C_ℓ) of the DGSE quantifies the fluctuations in the magnetic field and in the electron density of the turbulent interstellar medium of our Galaxy (e.g. Waelkens, Schekochihin & Enßlin 2009; Lazarian & Pogosyan 2012; Iacobelli et al. 2013).

★ Email: samir11@phy.iitkgp.ernet.in

There are several observations towards characterizing the DGSE spanning a wide range of frequency. Haslam et al. (1982) have measured the all-sky diffuse Galactic synchrotron radiation at 408 MHz. Reich (1982) and Reich & Reich (1988) have presented the Galactic synchrotron maps at a relatively higher frequency (1420 MHz). Using the 2.3 GHz Rhodes Survey, Giardino et al. (2001) have shown that the C_ℓ of the diffuse Galactic synchrotron radiation behaves like a power law ($C_\ell \propto \ell^{-\beta}$) where the power-law index $\beta = 2.43$ in the ℓ range $2 \leq \ell \leq 100$. Giardino et al. (2002) have found that the value of β is 2.37 for the 2.4 GHz Parkes Survey in the ℓ range $40 \leq \ell \leq 250$. The C_ℓ measured from the *Wilkinson Microwave Anisotropy Probe* (*WMAP*) data show a slightly lower value of β ($C_\ell \propto \ell^2$) for $\ell < 200$ (Bennett et al. 2003). Bernardi et al. (2009) have analysed 150 MHz Westerbork Synthesis Radio Telescope observations to characterize the statistical properties of the diffuse Galactic emission and find that

$$C_\ell = A \times \left(\frac{1000}{l}\right)^{\beta} \mathrm{mK}^2, \tag{1}$$

where $A = 253\,\mathrm{mK}^2$ and $\beta = 2.2$ for $\ell \leq 900$. Ghosh et al. (2012) have used GMRT 150 MHz observations to characterize the foregrounds for 21-cm experiments and find that $A = 513\,\mathrm{mK}^2$ and $\beta = 2.34$ in the ℓ range $253 \leq \ell \leq 800$. Recently, Iacobelli et al. (2013) present the first LOFAR detection of the DGSE around 160 MHz. They reported that the C_ℓ of the foreground synchrotron fluctuations is approximately a power law with a slope $\beta \approx 1.8$ up to angular multipoles of 1300.

In this Letter, we study the statistical properties of the DGSE using two fields observed by the TIFR GMRT Sky Survey (TGSS[1]; Sirothia et al. 2014). We have used the data that were calibrated and processed by Intema et al. (2016). We have applied the Tapered Gridded Estimator (TGE; Choudhuri et al. 2016a, hereafter Paper I) to the residual data to measure the C_ℓ of the background sky signal after point source subtraction. The TGE suppresses the contribution from the residual point sources in the outer region of the telescope's field of view (FoV) and also internally subtracts out the noise bias to give an unbiased estimate of C_ℓ (Choudhuri et al. 2016b). For each field, we are able to identify an angular multipole range where the measured C_ℓ is likely dominated by the DGSE and we present power-law fits for these.

2 DATA ANALYSIS

The TGSS survey contains 2000 h of observing time divided on 5336 individual pointings on an approximate hexagonal grid. The observing time for each field is about 15 min. For the purpose of this Letter, we have used only two data sets for two fields located at Galactic coordinates (9°, +10°; **Data1**) and (15°, −11°; **Data2**). We have selected these fields because they are close to the Galactic plane and also the contributions from the very bright compact sources are much less in these fields. The central frequency of this survey is 147.5 MHz with an instantaneous bandwidth of 16.7 MHz, which is divided into 256 frequency channels. All the TGSS raw data were analysed with a fully automated pipeline based on the SPAM package (Intema et al. 2009; Intema 2014). The operation of the SPAM package is divided into two parts: (a) pre-processing and (b) main pipeline. The pre-processing step calculates good-quality instrumental calibration from the best available scans on one of the primary calibrators and transfers these to the target field. In the main pipeline, the direction-independent and direction-dependent calibrations are calculated for each field and the calibrated visibilities are converted into 'CLEANed' deconvolved radio images. The off-source rms noise (σ_n) for the continuum images of these fields are 4.1 and 3.1 mJy beam^{-1} for **Data1** and **Data2**, respectively; both values lie close to the median rms noise of 3.5 mJy beam^{-1} for the whole survey. The angular resolution of these observations is 25 × 25 arcsec. This pipeline applies direction-dependent gains to image and subtract point sources to a $S_c = 5\,\sigma_n$ flux threshold covering an angular region of radius ∼1.5 times the telescope's FoV (3.1° × 3.1°) and also includes a few bright sources even further away. The subsequent analysis here uses the residual visibility data after subtracting out the discrete sources.

We have used the TGE to estimate C_ℓ from the measured visibilities $\mathcal{V}_i$ with $\boldsymbol{U}_i$ referring to the corresponding baseline. As mentioned earlier, the TGE suppresses the contribution from the residual point sources in the outer region of the telescope's FoV and also internally subtracts out the noise bias to give an unbiased estimate of C_ℓ (see details in Choudhuri et al. 2014, 2016b, Paper I). The tapering is introduced by multiplying the sky with a Gaussian window function $\mathcal{W}(\theta) = e^{-\theta^2/\theta_w^2}$. The value of θ_w should be chosen in such a way that it cuts off the sky response well before the first null of the primary beam without removing too much of the signal from the central region. Here, we have used $\theta_w = 95$ arcmin, which is slightly smaller than 114 arcmin, the half width at half maxima (HWHM) of the GMRT primary beam at 150 MHz. This is implemented by dividing the *uv* plane into a rectangular grid and evaluating the convolved visibilities $\mathcal{V}_{cg}$ at every grid point g

$$\mathcal{V}_{cg} = \sum_i \tilde{w}(\boldsymbol{U}_g - \boldsymbol{U}_i)\,\mathcal{V}_i, \tag{2}$$

where $\tilde{w}(\boldsymbol{U})$ is the Fourier transform of the taper window function $\mathcal{W}(\theta)$ and $\boldsymbol{U}_g$ refers to the baseline of different grid points. The entire data containing visibility measurements in different frequency channels that spans a 16 MHz bandwidth were collapsed to a single grid after scaling each baseline to the appropriate frequency.

The self-correlation of the gridded and convolved visibilities (equations (10) and (13) of Paper I) can be written as,

$$\langle \mid \mathcal{V}_{cg} \mid^2 \rangle = \left(\frac{\partial B}{\partial T}\right)^2 \int \mathrm{d}^2U \mid \tilde{K}\left(\boldsymbol{U}_g - \boldsymbol{U}\right) \mid^2 C_{2\pi U_g} + \sum_i \mid \tilde{w}(\boldsymbol{U}_g - \boldsymbol{U}_i) \mid^2 \langle \mid \mathcal{N}_i \mid^2 \rangle, \tag{3}$$

where $\left(\frac{\partial B}{\partial T}\right)$ is the conversion factor from brightness temperature to specific intensity, $\mathcal{N}_i$ is the noise contribution to the individual visibility $\mathcal{V}_i$ and $\tilde{K}\left(\boldsymbol{U}_g - \boldsymbol{U}\right)$ is an effective 'gridding kernel' that incorporates the effects of (a) telescope's primary beam pattern, (b) the tapering window function and (c) the baseline sampling in the *uv* plane.

We have approximated the convolution in equation (3) as,

$$\langle \mid \mathcal{V}_{cg} \mid^2 \rangle = \left[\left(\frac{\partial B}{\partial T}\right)^2 \int \mathrm{d}^2U \mid \tilde{K}(\boldsymbol{U}_g - \boldsymbol{U}) \mid^2\right] C_{2\pi U_g} + \sum_i \mid \tilde{w}(\boldsymbol{U}_g - \boldsymbol{U}_i) \mid^2 \langle \mid \mathcal{N}_i \mid^2 \rangle, \tag{4}$$

under the assumption that the $C_\ell\,(\ell = 2\pi \mid \boldsymbol{U} \mid)$ is nearly constant across the width of $\tilde{K}\left(\boldsymbol{U}_g - \boldsymbol{U}\right)$.

We define the TGE as

$$\hat{E}_g = M_g^{-1}\left(\mid \mathcal{V}_{cg} \mid^2 - \sum_i \mid \tilde{w}(\boldsymbol{U}_g - \boldsymbol{U}_i) \mid^2 \mid \mathcal{V}_i \mid^2\right), \tag{5}$$

[1] http://tgss.ncra.tifr.res.in

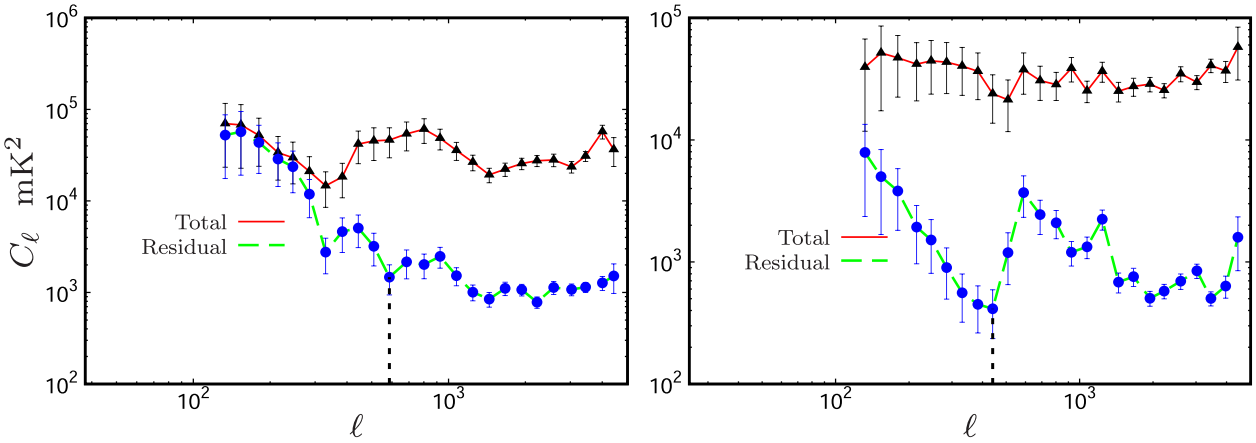

Figure 1. Estimated angular power spectra (C_ℓ) with $1-\sigma$ analytical error bars. The left and right panels are for **Data1** and **Data2**, respectively. The upper and lowers curves are before and after point source subtraction, respectively. The vertical dotted lines in both the panels show $\ell_{\rm max}$ beyond which ($\ell > \ell_{\rm max}$) the residual C_ℓ is dominated by the unsubtracted point sources.

where $M_{\rm g}$ is the normalizing factor that we have calculated by using simulated visibilities corresponding to a unit angular power spectrum (see details in Paper I). We have $\langle \hat{E}_{\rm g} \rangle = C_{\ell_{\rm g}}$, i.e. the TGE $\hat{E}_{\rm g}$ provides an unbiased estimate of the angular power spectrum C_ℓ at the angular multipole $\ell_{\rm g} = 2\pi U_{\rm g}$ corresponding to the baseline $\boldsymbol{U}_{\rm g}$. We have used the TGE to estimate C_ℓ and its variance in bins of equal logarithmic interval in ℓ (equations (19) and (25) in Paper I).

3 RESULTS AND CONCLUSIONS

The upper curves of the left- and right-hand panels of Fig. 1 show the estimated C_ℓ before point source subtraction for **Data1** and **Data2**, respectively. We find that for both the data sets the measured C_ℓ is in the range 10^4–10^5 mK^2 across the entire ℓ range. Model predictions (Ali et al. 2008) indicate that the point source contribution is expected to be considerably larger than the Galactic synchrotron emission across much of the ℓ range considered here, however, the two may be comparable at the smaller ℓ values of our interest. Further, the convolution in equation (3) is expected to be important at small ℓ and it is necessary to also account for this. The lower curves of both the panels of Fig. 1 show the estimated C_ℓ after point source subtraction. We see that removing the point sources causes a very substantial drop in the C_ℓ measured at large ℓ. This clearly demonstrates that the C_ℓ at these angular scales was dominated by the point sources prior to their subtraction. We further believe that after point source subtraction the C_ℓ measured at large ℓ continues to be dominated by the residual point sources that are below the threshold flux. The residual flux from imperfect subtraction of the bright sources possibly also makes a significant contribution in the measured C_ℓ at large ℓ. This interpretation is mainly guided by the model predictions (fig. 6 of Ali et al. 2008) and is also indicated by the nearly flat C_ℓ, which is consistent with the Poisson fluctuations of a random point source distribution. In contrast to this, C_ℓ shows a steep power-law ℓ dependence at small ℓ ($\leq \ell_{\rm max}$) with $\ell_{\rm max} = 580$ and 440 for **Data1** and **Data2**, respectively. This steep power law is the characteristic of the diffuse Galactic emission and we believe that the measured C_ℓ is possibly dominated by the DGSE at the large angular scales corresponding to $\ell \leq \ell_{\rm max}$. As mentioned earlier, the convolution in equation (3) is expected to be important at large angular scales and it is necessary to account for this in order to correctly interpret the results at small ℓ.

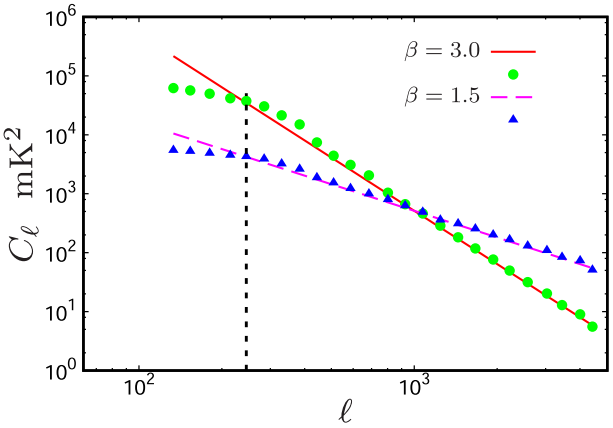

Figure 2. Comparison between the estimated C_ℓ and the model C_ℓ^M using simulation for **Data1**. The data points and the lines are for the estimated C_ℓ and the input model C_ℓ^M (with $\beta = 1.5$ and 3), respectively. We see that the convolution is important in the range $\ell < \ell_{\rm min} = 240$ shown by the vertical dashed line and we have excluded this region from our subsequent analysis. The estimated C_ℓ matches closely with C_ℓ^M in the range $\ell \geq \ell_{\rm min}$, which we have used for our analysis.

We have carried out simulations in order to assess the effect of the convolution on the estimated C_ℓ. GMRT visibility data were simulated assuming that the sky brightness temperature fluctuations are a realization of a Gaussian random field with input model angular power spectrum C_ℓ^M of the form given by equation (1). The simulations incorporate the GMRT primary beam pattern and the *uv* tracks corresponding to the actual observation under consideration. The reader is referred to Choudhuri et al. (2014) for more details of the simulations. Fig. 2 shows the C_ℓ estimated from the **Data1** simulations for $\beta = 3$ and 1.5 which roughly encompasses the entire range of the power-law index we expect for the Galactic synchrotron emission. We find that the effect of the convolution is important in the range $\ell < \ell_{\rm min} = 240$ and we have excluded this ℓ range from our analysis. We are, however, able to recover the input model angular power spectrum quite accurately in the region $\ell \geq \ell_{\rm min}$ which we have used for our subsequent analysis. We have also carried out the same analysis for **Data2** (not shown here) where we find that $\ell_{\rm min}$ has a value that is almost the same as for **Data1**.

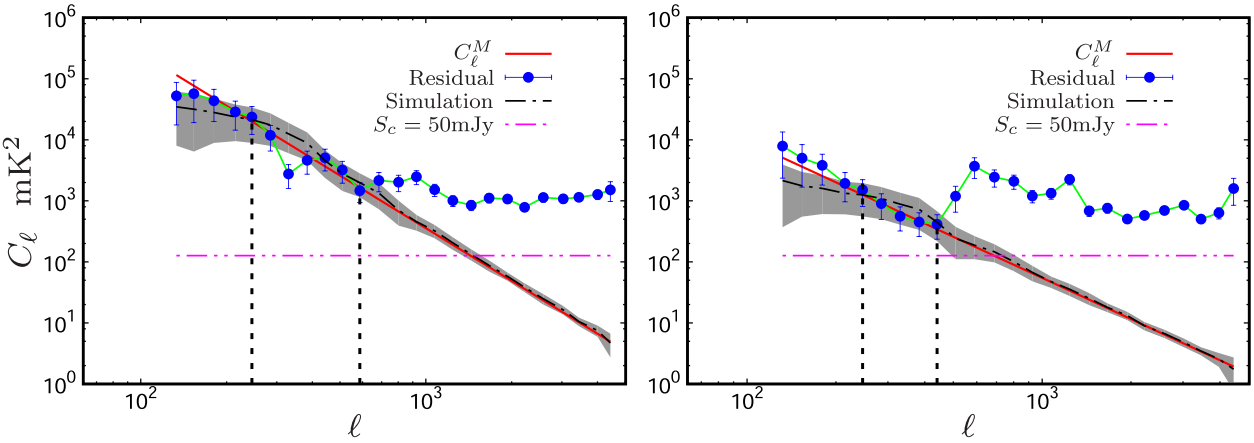

Figure 3. Estimated angular power spectra (C_ℓ) using residual data. The left- and right-hand panels refer to **Data1** and **Data2**, respectively. The solid circles with $1-\sigma$ error bars show C_ℓ estimated from the residual data, the vertical dashed lines show the $\ell_{\rm min} - \ell_{\rm max}$ range used for fitting a power-law model and the solid lines show the best-fitting model. The dash-dot lines with the $1-\sigma$ shaded region show the mean and standard deviation of C_ℓ estimated from 128 realizations of simulations with the best-fitting power law as input model. The dot-dot–dashed horizontal lines show C_ℓ predicted from the residual point sources below a threshold flux density $S_c = 50$ mJy. Note that for **Data2** the estimated values are only upper limits on the DGSE power spectrum (see Section 3).

Table 1. This shows the values of the parameters that are used to fit the data. In comparison, the parameters from other observations are also shown in this table. For **Data2**, the best-fitting values are derived with the assumption that the residual contribution is negligible below $\ell_{\rm max}$.

	Galactic coordinate (l, b)	$\ell_{\rm min}$	$\ell_{\rm max}$	A (mK^2)	β	N	$\chi^2/(N-2)$
Data1	(9°, +10°)	240	580	356 ± 109	2.8 ± 0.3	6[a]	0.33
Data2	(15°, −11°)	240	440	54 ± 26	2.2 ± 0.4	5	0.15
Bernardi et al. (2009)	(137°, +8°)	100	900	253 ± 40	2.2 ± 0.3	–	–
Ghosh et al. (2012)	(151.8°, +13.89°)	253	800	513 ± 41	2.34 ± 0.28	–	–
Iacobelli et al. (2013)	(137°, +7°)	100	1300	–	1.84 ± 0.19	–	–
	(−, ≥ + 10°)	–	–	175[b]	2.88	–	–
	(−, ≤ − 10°)	–	–	212[b]	2.74	–	–
	(−, ≥ + 20°)	–	–	85[b]	2.88	–	–
La Porta et al. (2008)	(−, ≤ − 20°)	–	–	50[b]	2.83	–	–
	(−, ≥ + 10°)	–	–	691[c]	2.80	–	–
	(−, ≤ − 10°)	–	–	620[c]	2.70	–	–
	(−, ≥ + 20°)	–	–	275[c]	2.83	–	–
	(−, ≤ − 20°)	–	–	107[c]	2.87	–	–

Notes. [a]Excluding one outlier point;
[b]Extrapolated from 1420 to 147.5 MHz;
[c]Extrapolated from 408 to 147.5 MHz.

We have used the ℓ range $\ell_{\rm min} \le \ell \le \ell_{\rm max}$ to fit a power law of the form given in equation (1) to the C_ℓ measured after point source subtraction. The data points with $1-\sigma$ error bars and the best-fitting power law are shown in Fig. 3. Note that we have identified one of the **Data1** points as an outlier and excluded it from the fit. The best-fitting parameters (A, β), N the number of data points used for the fit and $\chi^2/(N-2)$ the chi-square per degree of freedom (reduced χ^2) are listed in Table 1. The rather low values of the reduced χ^2 indicate that the errors in the measured C_ℓ have possibly been somewhat overestimated. In order to validate our methodology, we have simulated the visibility data for an input model power spectrum with the best-fitting values of the parameters (A, β) and used this to estimate C_ℓ. The mean C_ℓ and $1-\sigma$ errors (shaded region) estimated from 128 realization of the simulation are shown in Fig. 3. For the relevant ℓ range we find that the simulated C_ℓ is in very good agreement with the measured values thereby validating the entire fitting procedure. The horizontal lines in both the panels of Fig. 3 show the C_ℓ predicted from the Poisson fluctuations of residual point sources below a threshold flux density of $S_c = 50$ mJy. The C_ℓ prediction here is based on the 150 MHz source counts of Ghosh et al. (2012). We find that for $\ell > \ell_{\rm max}$ the measured C_ℓ values are well in excess of this prediction indicating that (1) there are significant residual imaging artefacts around the bright source ($S > S_c$) which were subtracted and/or (2) the actual source distribution is in excess of the predictions of the source counts. Note that the actual S_c values (20.5 and 15.5 mJy for **Data1** and **Data2**, respectively) are well below 50 mJy, and the corresponding C_ℓ predictions will lie below the horizontal lines shown in Fig. 3.

For both the fields C_ℓ (Fig. 3) is nearly flat at large ℓ (> 500) and it is well modelled by a power law at smaller ℓ ($240 \le \ell \lesssim 500$). For **Data1**, the power law rises above the flat C_ℓ and the power law is likely dominated by the DGSE. However, for **Data2**, the power law falls below the flat C_ℓ and it is likely that in addition to the DGSE there is a significant residual point sources contribution. For **Data2**, we interpret the best-fitting power law as an upper limit for the DGSE.

The best-fitting parameters $(A, \beta) = (356.23 \pm 109.5, 2.8 \pm 0.3)$ and $(54.6 \pm 26, 2.2 \pm 0.4)$ for **Data1** and **Data2**, respectively, are compared with measurements from other 150 MHz observations such as Bernardi et al. (2009), Ghosh et al. (2012), Iacobelli et al. (2013) in Table 1. Further, we have also used an earlier work (La Porta et al. 2008) at higher frequencies (408 and 1420 MHz) to estimate and compare the amplitude of the angular power spectrum of the DGSE expected at our observing frequency. Using the best-fitting parameters (tabulated at $\ell = 100$) at 408 and 1420 MHz, we extrapolate the amplitude of the C_ℓ at our observing frequency at $\ell = 1000$ for $|b| \geq 10^\circ$ and $|b| \geq 20^\circ$. In this extrapolation, we use a mean frequency spectral index of $\alpha = 2.5$ (de Oliveira-Costa et al. 2008) ($C_\ell \propto \nu^{2\alpha}$). The extrapolated amplitude values are shown in Table 1. In Table 1, we note that the angular power spectra of the DGSE in the Northern hemisphere are comparatively larger than those of the Southern hemisphere. The best-fitting parameter A for **Data1**(**Data2**) agrees mostly with the extrapolated values obtained from $b \geq +10^\circ$ ($b \leq -10^\circ$) and $b \geq +20^\circ$($b \leq -20^\circ$) within a factor of about 2 (4). The best-fitting parameter β for **Data1** and **Data2** is within the range of 1.5–3.0 found by all the previous measurements at 150 MHz and higher frequencies.

The entire analysis here is based on the assumption that the DGSE is a Gaussian random field. This is possibly justified for the small patch of the sky under observation given that the diffuse emission is generated by a random process like MHD turbulence. The estimated C_ℓ remains unaffected even if this assumption breaks down, only the error estimates will be changed. We note that the parameters (A, β) are varying significantly from field to field across the different directions in the sky. We plan to extend this analysis for the whole sky and study the variation of the amplitude (A) and power-law index (β) of C_ℓ using the full TGGS survey in future.

ACKNOWLEDGEMENTS

We thank an anonymous referee for helpful comments. S. Choudhuri would like to acknowledge the University Grant Commission, India, for providing financial support. AG would like to acknowledge Postdoctoral Fellowship from the South African Square Kilometre Array Project for financial support. We thank the staff of the GMRT that made these observations possible. GMRT is run by the National Centre for Radio Astrophysics of the Tata Institute of Fundamental Research.

REFERENCES

Ali S. S., Bharadwaj S., Chengalur J. N., 2008, MNRAS, 385, 2166
Bennett C. L. et al., 2003, ApJS, 148, 97
Bernardi G. et al., 2009, A&A, 500, 965
Bharadwaj S., Ali S. S., 2005, MNRAS, 356, 1519
Bowman J. D. et al., 2013, PASA, 30, e031
Choudhuri S., Bharadwaj S., Ghosh A., Ali S. S., 2014, MNRAS, 445, 4351
Choudhuri S., Bharadwaj S., Chatterjee S., Ali S. S., Roy N., Ghosh A., 2016a, MNRAS, 463, 4093 (Paper I)
Choudhuri S., Bharadwaj S., Roy N., Ghosh A., Ali S. S., 2016b, MNRAS, 459, 151
de Oliveira-Costa A., Tegmark M., Gaensler B. M., Jonas J., Landecker T. L., Reich P., 2008, MNRAS, 388, 247
Furlanetto S. R., Oh S. P., Briggs F. H., 2006, Phys. Rep., 433, 181
Ghosh A., Bharadwaj S., Ali S. S., Chengalur J. N., 2011a, MNRAS, 411, 2426
Ghosh A., Bharadwaj S., Ali S. S., Chengalur J. N., 2011b, MNRAS, 418, 2584
Ghosh A., Prasad J., Bharadwaj S., Ali S. S., Chengalur J. N., 2012, MNRAS, 426, 3295
Giardino G., Banday A. J., Fosalba P., Górski K. M., Jonas J. L., O'Mullane W., Tauber J., 2001, A&A, 371, 708
Giardino G., Banday A. J., Górski K. M., Bennett K., Jonas J. L., Tauber J., 2002, A&A, 387, 82
Haslam C. G. T., Salter C. J., Stoffel H., Wilson W. E., 1982, A&AS, 47, 1
Iacobelli M. et al., 2013, A&A, 558, A72
Intema H. T., 2014, preprint (arXiv:1402.4889)
Intema H. T., van der Tol S., Cotton W. D., Cohen A. S., van Bemmel I. M., Röttgering H. J. A., 2009, A&A, 501, 1185
Intema H. T., Jagannathan P., Mooley K. P., Frail D. A., 2016, A&A, 598, A78
Koopmans L. et al., 2015, in Bourke T. L. et al., eds, Proc. Sci., The Cosmic Dawn and Epoch of Reionisation with SKA. SISSA, Treiste, PoS(AASKA14)001
La Porta L., Burigana C., Reich W., Reich P., 2008, A&A, 479, 641
Lazarian A., Pogosyan D., 2012, ApJ, 747, 5
Morales M. F., Wyithe J. S. B., 2010, ARAA, 48, 127
Neben A. R. et al., 2016, ApJ, 826, 199
Parsons A. R. et al., 2010, AJ, 139, 1468
Pritchard J. R., Loeb A., 2012, Rep. Prog. Phys., 75, 086901
Reich W., 1982, A&AS, 48, 219
Reich P., Reich W., 1988, A&AS, 74, 7
Shaver P. A., Windhorst R. A., Madau P., de Bruyn A. G., 1999, A&A, 345, 380
Sirothia S. K., Lecavelier des Etangs A., Gopal-Krishna, Kantharia N. G., Ishwar-Chandra C. H., 2014, A&A, 562, A108
Swarup G., Ananthakrishnan S., Kapahi V. K., Rao A. P., Subrahmanya C. R., Kulkarni V. K., 1991, Curr. Sci., 60, 95
van Haarlem M. P. et al., 2013, A&A, 556, A2
Waelkens A. H., Schekochihin A. A., Enßlin T. A., 2009, MNRAS, 398, 1970

This paper has been typeset from a TEX/LATEX file prepared by the author.